Ji et al. *NPG Asia Materials* (2018) 10: 749–760
DOI 10.1038/s41427-018-0070-1

NPG Asia Materials

ARTICLE Open Access

Lightweight and flexible electrospun polymer nanofiber/metal nanoparticle hybrid membrane for high-performance electromagnetic interference shielding

He Ji[1], Rui Zhao[1], Nan Zhang[1], Changxian Jin[2], Xiaofeng Lu[1] and Ce Wang[1]

Abstract

To resist the increasingly serious radiation pollution, there is a great need for the fabrication of high-performance electromagnetic interference (EMI) shielding materials. However, it is a great challenge to prepare EMI shielding materials with high efficiency, lightweight, and flexibility for practical applications. Here, we demonstrate an efficient and facile approach to prepare freestanding, lightweight, and flexible crosslinking polyacrylonitrile (CPAN) nanofiber (NF)/metal nanoparticle (MNP) hybrid membranes with a high efficiency and reasonable strength via electrospinning followed by an electroless deposition process. In contrast to a Cu- and Ni-decorated CPAN NF membrane, the resultant CPAN NF/Ag nanoparticle (NP) hybrid membrane exhibited much better electrical conductivity. Furthermore, a superior EMI shielding effectiveness of ≈90 dB is achieved for the lightweight CPAN NF/Ag NP hybrid membrane (53 μm), which is superior to pure metal and most of the synthesized EMI shielding materials. The excellent EMI shielding efficiency is attributed to the high conductivity of MNPs and favorable porous structure in the hybrid NF membrane. In addition, the resultant CPAN NF/MNP hybrid membrane shows a reasonable mechanical strength and excellent flexibility. The prepared polymer NF/MNP hybrid membrane shows promising applications in smart portable and wearable electronics.

Introduction

With the rapid progress of modern electronics and telecommunications packed with large integrated circuits, an increasingly dense and intensive electromagnetic interference (EMI) of radio frequency radiation has been become a new and serious pollutant source in addition to noise, water, and air pollution, which leads to great trouble for highly sensitive electronic equipment as well as the surrounding environment. To tackle the problem, great efforts have been made for the development of high-performance EMI shielding material (EMI SM) that can effectively shield high energy and broadband radiation[1–5]. Generally, an effective EMI shielding material is dominated by three main functions: reflection, absorption, and multi-reflection[1,6,7]. Reflection usually occurs on the surface of conductive materials because the incoming electromagnetic (EM) waves would interact with mobile charge carriers (electrons or holes). When EM radiation interacts with electrical or magnetic dipoles of shielding material, it will be absorbed and turn into heat energy. Therefore, EMI shielding material should be thick enough to dissipate more radiation. Both the reflection and absorption performance of the EMI shielding materials are dependent on the high electrical conductivity. Multi-reflection is attributed to the EM wave reflection and scattering at various inhomogeneous interfaces inside the EMI shielding material, which has recently been found to contribute to EMI shielding effectiveness[3,8,9].

Correspondence: Xiaofeng Lu (xflu@jlu.edu.cn) or Ce Wang (cwang@jlu.edu.cn)
[1]Alan G. MacDiarmid Institute, College of Chemistry, Jilin University, Changchun 130012, China
[2]Jilin Zhenliang Science and Technology Co. Ltd, Changchun 130012, China

Metal shrouds are well known to be a good choice as EMI shielding materials due to their high electrical conductivity[4–7]. However, metal shrouds suffer from poor mechanical flexibility and exceedingly high weight for practical applications. However, the lightweight and flexibility of the EMI shielding materials are the two important technical requirements in addition to the high effectiveness needed for effective and practical applications in smart electronic devices, aircraft, and aerospace fields. To achieve this object, extensive work has been done to study polymer matrix composites with embedded conductive fillers for EMI shielding, including a silver nanowire-polyimide hybrid[10,11], MXene-polymer composites[3], graphene-polymer nanocomposites[12], and polypropylene–stainless-steel fiber composites[13]. In these systems, the intrinsic conductivity, dispersion, distribution, and orientation of the fillers have significant influence on the EMI shielding performance[14]. In most cases, a low content of conductive fillers leads to a poor conductivity of the polymer matrix composites, while a high content of conductive fillers usually results in inferior mechanical properties and processibility due to the severe agglomeration of the fillers. In addition, for most of the polymer-conductive filler hybrids, the low thermal conductivity, poor heat resistance, ease of aging, and relatively high thickness usually restrict their applications in the smart and small-scale electronics fields. Therefore, it is highly desirable to develop polymer matrix composites with uniform dispersions of conductive fillers and strong interfacial interactions between the polymer and conductive fillers.

Recently, foam structures with a high porosity have attracted more and more attention as EMI shielding materials due to their high specific shielding effectiveness (SSE)[15–17]. For example, an SSE of 1148 dB cm^3 g^{-1} in the X-band with a low density of ≈0.02 g cm^{-3} and a thickness of 2.3 mm was achieved for the porous multi-walled carbon nanotube (CNT) water-borne polyurethane composite foam[18]. However, it is still a great challenge to increase the shielding effectiveness (SE), especially at a smaller thickness. The electrospinning technique is a simple and versatile approach to prepare porous foam-like freestanding polymer membranes consisting of nanofibers (NFs) with the feature of a large specific surface area, high porosity, and good interconnectivity, providing a potential effective platform for the absorption and multi-reflection of the electromagnetic wave inside the materials. Combining with an easy post-treatment method, conductive fillers could be regularly and closely distributed on individual fibers, offering interlaced and interconnected highly conductive 3D networked highways for electron transport, implying their superior shielding performance at a smaller thickness. Due to a large amount of reflecting surface between the fibers, the electrospun nanofiber membrane possesses the ability to behave as a multilevel shielding material. In addition, the interfacial polarization between the conductive materials and polymer improves the polarization loss of the electrospun nanofiber-based hybrid membranes to the incident wave[18]. Therefore, electrospun nanofiber-based hybrid membranes show great potential as lightweight, flexible, and ultrahigh-performance shielding materials.

Here, we report a highly flexible porous electrospun polymer NF decorated with a metal (Ag, Cu, Ni) nanoparticle (NP) membrane with an excellent EMI shielding performance. All freestanding hybrid membranes are fabricated via electrospinning followed by an electroless deposition process (Fig. 1a). In particular, the as-prepared crosslinked polyacrylonitrile (CPAN) nanofiber (NF)/Ag NP hybrid membrane exhibited an extraordinary EMI SE of ~90 dB with a thickness of ~53 μm. In addition, these CPAN/metal NP (MNP) hybrid membranes possess other advantages such as easy processing, lightweight, and mechanical flexibility. To the best of our knowledge, the reported EMI SE values are among the best values of synthetic EMI shielding materials with similar or larger thickness and are also higher than the reported EMI SE values of the typical pure metals. This work offers a new method for the development of a large variety of high-performance EMI shielding materials.

Materials and methods

Materials

Polyacrylonitrile (PAN, $M_w = 80{,}000$) was purchased from Jilin Carbon Group, Jilin, China. Silver nitrate ($AgNO_3$, 99%), copper sulfate ($CuSO_4$, 99%), nickel sulfate hexahydrate ($NiSO_4{\cdot}6H_2O$, 99%), citric acid ($C_6H_8O_7$), sodium pyrophosphate ($Na_4P_2O_7{\cdot}10H_2O$), and sodium potassium tartrate ($KNaC_4H_4O_6{\cdot}4H_2O$) were purchased from Sinopharm Chemical Reagent Corporation. Dimethyl formamide (DMF) and ethylenediamine ($C_2H_8N_2$) were purchased from Tianjin Tiantai Refined Chemicals Co., Ltd. Sodium hydroxide (NaOH), ethanol (C_2H_6O), ethylene glycol ($C_2H_4O_2$), ammonia solution (NH_3, 25%), isopropyl alcohol (IPA), formaldehyde (HCHO, 36%), and polyvinylalcohol (PVA, $M_w = 6{,}000$) were purchased from Beijing Chemical Works. Polyvinylpyrrolidone (PVP, $M_w = 1{,}300{,}000$) was purchased from Alfa Aesar. Dimethylamine-borane (DMAB) was purchased from Sigma Aldrich. All the reagents were used without further purification.

Preparation of PAN NF membrane via an electrospinning technique

In a typical synthetic procedure, 1.50 g of PAN was dissolved in 17.25 g of DMF, followed by vigorous stirring for 6 h at 75 °C to form a homogeneous and viscous solution. After cooling to room temperature, the spinning

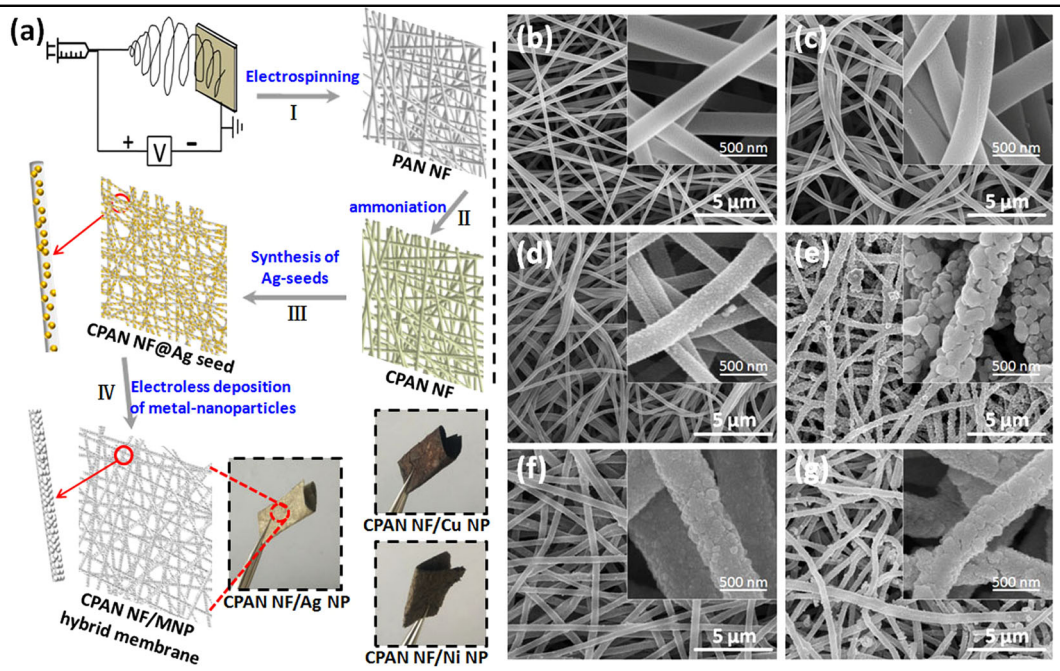

Fig. 1 Fabrication and morphologies of the CPAN NF/MNP hybrid nanofiber membranes. a Schematic representation of the procedure for the fabrication of CPAN NF/MNP hybrid nanofiber membranes. FE-SEM images of (**b**) the as-electrospun PAN NF membranes, **c** CPAN NF membranes, **d** CPAN NF@Ag seed, **e** CPAN NF/Ag NP, **f** CPAN NF/Cu NP, and **g** CPAN NF/Ni NP. The inset images in (**b**–**g**) are their corresponding magnified SEM images

solution was carefully put into a glass capillary (the diameter of the spinning jet is 1.5 mm) and connected to a positive electrode of a high-voltage power supply (Gamma High Voltage Research, Ormond Beach, FL, USA; dc power supply). A 20-cm work distance between the spinning tip and the ground collector and 15 kV of the applied voltage were used for electrospinning. Finally, the PAN membranes were maintained in a vacuum at 65 °C for 12 h to remove any possible solvent residue.

Preparation of CPAN NF membrane

CPAN NF membranes were synthesized based on an amination reaction. The prepared PAN NFs (0.65 g), ethylenediamine (0.30 mL), and ethylene glycol (50 mL) were added to a 100 mL round bottomed flask. The reaction was carried out at 135 °C in an oil bath. After 1 h, the obtained CPAN NF membranes were washed with warm deionized water and dried in a vacuum oven at 65 °C for 12 h.

Synthesis of Ag seeds on the surface of individual CPAN NFs

The CPAN NF membranes obtained (4 cm × 4 cm) were first immersed in silver-ammonia solution (0.8 g $AgNO_3$, 6 mL $NH_3{\cdot}H_2O$, 80 mL ethanol) for 8 h. After washing with ethanol, the CPAN NF membranes were then put into a 100-mL round-bottom flask containing 80 mL of ethanol and 2 g of PVP. The mixed solution was kept under mechanical stirring at 70 °C for 3 h. After washing with ethanol and drying at 65 °C for 12 h, the CPAN NF membranes with Ag seeds (hereafter, CPAN NF@Ag seed) were obtained.

Electroless deposition of MNPs onto CPAN NFs

Electroless deposition of Ag NPs

CPAN NF@Ag seed membranes (4×2 cm) were put in a 30 mL $Ag(NH_3)_2^+$ solution (20 g L^{-1} $AgNO_3$) mixed with 0.36 g of citric acid under general mechanical stirring. Then, the reducing agent consisting of 3 g of KNa-$C_4H_4O_6{\cdot}4H_2O$ in 30 mL of deionized water was added slowly into the above mixture. Electroless deposition continued for a time ranging from 30 to 120 min under gentle stirring at room temperature. Finally, the prepared CPAN NF/Ag NP hybrid membrane was taken out of the electroless deposition bath, rinsed thoroughly with DI water and dried in a vacuum oven at 65 °C for 12 h. The samples obtained will be denoted as CPAN NF/Ag NP-*x*, where *x* stands for the different electroless plating times.

Electroless deposition of Cu NPs

CPAN NF@Ag seed membranes (4×2 cm) were put into a flask containing 60 mL of aqueous solution consisting of 0.60 g of $CuSO_4$, 0.25 mL of 5 wt% PVA aqueous solution,

0.96 g of $KNaC_4H_4O_6{\cdot}4H_2O$, 0.58 g of NaOH, and 0.60 mL of HCHO. The electroless plating was allowed to continue for 120 min under gentle stirring at room temperature. Finally, the prepared CPAN NF/Cu NP hybrid membrane was taken out of the electroless deposition bath, rinsed thoroughly with DI water and dried in a vacuum oven at 65 °C for 12 h.

Electroless deposition of Ni NPs

CPAN NF@Ag seed membranes (4×2 cm) were put into a flask containing 60 mL of aqueous solution consisting of 0.45 g $NiSO_4{\cdot}6H_2O$, 0.45 g $Na_4P_2O_7{\cdot}10H_2O$, 0.56 mL $NH_3{\cdot}H_2O$, and 0.027 g DMAB. The electroless plating continued for 120 min under gentle stirring at room temperature. Finally, the prepared CPAN NF/Ni NP hybrid membrane was removed from the electroless plating bath, rinsed thoroughly with DI water and dried in a vacuum oven at 65 °C for 12 h.

Characterization of materials

The morphology and microstructure of the as-prepared CPAN NF/MNP hybrids coated with a thin layer of platinum were investigated by field emission scanning electron microscopy (FE-SEM, FEI Nova NanoSEM) at an acceleration voltage of 15.0 kV. The phase and the crystallographic structure of the products were determined via X-ray diffraction analysis (XRD, PANalytical B.V. Empyrean) with Cu K_α radiation. The chemical composition of the shields were characterized using an X-ray photoelectron spectrometer (XPS, Thermo Scientific ESCALAB250), which uses Al K_α as the excitation source. The weight percentage of Ag, Cu, and Ni by the electroless deposition process in the CPAN NF/MNP hybrid membrane was detected by inductively coupled plasma atomic emission spectrometry (ICP-AES, Agilent 725). The mechanical properties of the hybrid membranes (width = 10 mm) were evaluated by using an AGS-H tensile tester (Shimadzu Corporation, Kyoto, Japan) with a rate of grip separation of 3 mm·min^{-1} and a gauge length of 20 mm. The tensile strength and elongation at break were evaluated using stress–strain curves. The density was calculated as the sample weight divided by the total volume of the hybrid membranes according to ASTM D328. The electrical conductivity (σ) of all hybrid membranes was determined using a classical four-point probe (RTS-2, Guangzhou Four Probe Technology Co., Ltd.) with a SourceMeter (Keithley 2400, United States). The inter-pin distance of the probe was 1.0 mm. The results were the average of at least five different regions of samples to ensure the accuracy of the electrical conductivity measurements. The pore size distribution and porosity of the nanofiber membranes were measured by using a capillary flow porometer (CFP-1100AI, Porous Materials Inc., USA) and a gravimetric method (isopropyl alcohol was used asthe wetting liquid), respectively.

EMI shielding characterization

The EMI shielding effectiveness was measured by the rectangular waveguide method using a 2-port network analyzer (AV3672B-S, China Electronics Technology Instruments Co., Ltd.) in the 8–26.5 GHz frequency range. The hybrid membrane was cut into a rectangular-shaped piece with dimensions slightly larger than 25×10.0 mm, 16×8 mm, and 11×4 mm to meet waveguide measurement with different frequency bands of the X-band (8–12.4 GHz), Ku-band (12–18 GHz), and K-band (18–26.5 GHz), respectively.

EMI SE was used to measure the ability of the material to attenuate the electromagnetic wave strength, which is defined as the logarithm of incoming power (P_i) to transmitted power (P_t) of an electromagnetic wave in decibels (dB). There are three typical processes when an electromagnetic wave propagates to a shielding material. Part of the electromagnetic wave is reflected on the surface of the material when interacting with charge carriers; part of the electromagnetic wave is absorbed and dissipated in the form of a leaking current or heat due to the interaction with the electric or magnetic dipoles of the material; part of the electromagnetic wave is multi-reflected inside the shielding material because of the interfaces or defect sites within the material; and the other electromagnetic waves penetrate through the material. Since multi-reflected waves get absorbed or dissipated as heat in the same way as the absorption mechanism, the total EMI shielding effectiveness (SE_T) is dominated by two functions: reflection (SE_R) and absorption (SE_A). Based on the description above, the total EMI SE (SE_T) can be written as

$$SE_T = SE_R + SE_A \tag{1}$$

The reflection coefficient (R), transmission coefficient (T), and absorption coefficient (A) were calculated by the S parameters (S_{11} and S_{21} or S_{12} and S_{22}) according to the following equations:

$$R = |S_{11}|^2 = |S_{22}|^2 \tag{2}$$

$$T = |S_{12}|^2 = |S_{21}|^2 \tag{3}$$

$$A = 1 - R - T \tag{4}$$

Effective absorbance (A_{eff}), the absorption efficiency for the electromagnetic wave that propagates in shield material, can bedescribed as

$$A_{eff} = (1 - R - T)/(1 - R) \tag{5}$$

Finally, SE_A, SE_R and SE_T are obtained by using following equations:

$$SE_R = 10log\left(\frac{1}{1-R}\right) = 10log\left(\frac{1}{1-|S_{11}|^2}\right) \quad (6)$$

$$SE_A = 10log\left(\frac{1}{1-A_{eff}}\right) = 10log\left(\frac{1-|S_{11}|^2}{|S_{21}|^2}\right) \quad (7)$$

$$SE_T = SE_R + SE_A = 10log\left(\frac{1}{|S_{21}|^2}\right) \quad (8)$$

Results and discussion

Figure 1a illustrates the fabrication process of the electrospun CPAN NF/MNP hybrid membranes. CPAN NF membranes were prepared via an electrospinning technique and post-treatment. The SEM image reveals that smooth and interlaced 3D networked PAN NFs with average diameters of 235 ± 4 nm were observed in the product of the PAN membrane with a white color (Fig. 1b). After the crosslinking reaction, the resultant CPAN fibers with a yellow color became more intertwined, and their average diameters increased slightly to 293 ± 3 nm, while their surfaces were still smooth (Fig. 1c). The crosslinking reaction between PAN NFs with ethylenediamine was confirmed by the FTIR spectra (Supplementary Information, Supplementary Figure S1a). The pure PAN NFs show typical –C≡N and C=O stretching peaks at 2244 and 1734 cm^{-1}. These peaks decreased significantly after the crosslinking reaction, and new peaks at 1566 and 1639 cm^{-1} corresponding to –NH bending motion combined with a –C = N stretching vibration of the C(=NH)–NH– group appeared, demonstrating the formation of the hydrazide group during the crosslinking reaction[19]. Then, Ag seeds were deposited on the surface of the electrospun CPAN NFs via the reduction of Ag^+ adsorbed on the surface of CPAN NFs through the amine groups by the reducing agent PVP. The formation of Ag seeds has also been clearly observed by the color change of the NF membranes from bright yellow to dark yellow, which has also been proved by the XRD pattern (Supplementary Figure S1b). Figure 1d clearly shows that the surfaces of the NFs were uniformly assembled with a large variety of spherical Ag seeds with diameters of 20–25 nm. Then, diverse metal (Ag, Cu, Ni) NPs were deposited on the surface of the CPAN NFs via an electroless plating process. The representative SEM images of CPAN NF/Ag NP, CPAN NF/Cu NP, and CPAN NF/Ni NP hybrid membranes show that almost the entire surface of these NFs is covered by a large number of hierarchical nanoclusters, which can be achieved by simple assembly of MNPs on the surface (Fig. 1e–g). The NFs coated with MNPs maintain their porous structures with average diameters of 365 ± 3, 366 ± 4, and 351 ± 2 nm, respectively. The diameters of the NFs obviously increased after the electroless deposition process, confirming the formation of Ag, Cu, and Ni NPs on the surface of NFs. The SEM images showed that MNPs were regularly and closely distributed on individual fibers, providing interlaced and interconnected highly conductive 3D networked highways for electron transport, implying their potential for EMI shielding applications. The formation of MNPs has also been proved by the X-ray diffraction (XRD) and X-ray photoelectron spectroscopy (XPS) analysis. The XRD spectrum of the CPAN NF/Ag NP, CPAN NF/Cu NP, and CPAN NF/Ni NP hybrid membranes revealed the formation of typical face-centered cubic structures of Ag, Cu, and Ni NPs in the hybrids (Fig. 2a). The XPS measurement provides further information regarding the chemical composition and oxidation state of the CPAN NF/MNP hybrid membranes. Two main peaks located at 368.0 and 374.0 eV are observed in the CPAN NF/Ag NP product, which can be assigned to Ag $3d_{5/2}$ and Ag $3d_{3/2}$, respectively, indicating the formation of metallic silver[20] (Fig. 2c, f). For the CPAN NF/Cu NP product, the main doubled Cu $2p_{3/2}$ peaks centered at 932.5 and 934.6 eV are attributed to Cu^+/Cu^0 and CuO, respectively[21]. The satellite peak is also observed at 944.0 eV, demonstrating the presence of the oxidation state of Cu[22] (Fig. 2d, g). A similar result has also been observed for the CPAN NF/Ni NP hybrid membrane. The nickel $2p_{3/2}$ binding energy at 856.1 eV and the intense satellite peak are the characteristics of Ni^{2+} in $Ni(OH)_2$/NiO, indicating a slight oxidation state of the Ni NPs[23](Fig. 2e, h).

The large conductivity is a critical factor for high electromagnetic shielding values, which is an intrinsic ability of a material to absorb EM radiation. Figure 2b presents the surface electrical conductivities of the prepared CPAN NF/Ag NP, CPAN NF/Cu NP, and CPAN NF/Ni NP hybrid membrane with similar metal layer thickness and membrane thickness. As the density of Ag is slightly larger than the density of Cu and Ni, the weight percentages of Ag, Cu, and Ni in the corresponding CPAN NF/MNP via the electroless deposition process show values of ~78.0%, 65.8%, and 65.0%, which are determined by the ICP-AES measurement. The electrical conductivities of the metalized NFs varied significantly for different types of metal. CPAN NF/Ag NP hybrid membranes exhibited the highest electrical conductivity among all the prepared NF membranes, reaching 5.6×10^4 S cm^{-1}. The excellent electrical conductivity of CPAN NF/Ag NP hybrid membranes should be attributed to the intrinsic high conductivity of Ag and the formation of continuous Ag components on the surface of CPAN NFs. By contrast, CPAN NF/Cu NP and CPAN NF/Ni NP hybrid membranes showed relatively low electrical conductivity with values of 6.4×10^3 and 1.3×10^3 S cm^{-1}, respectively. The

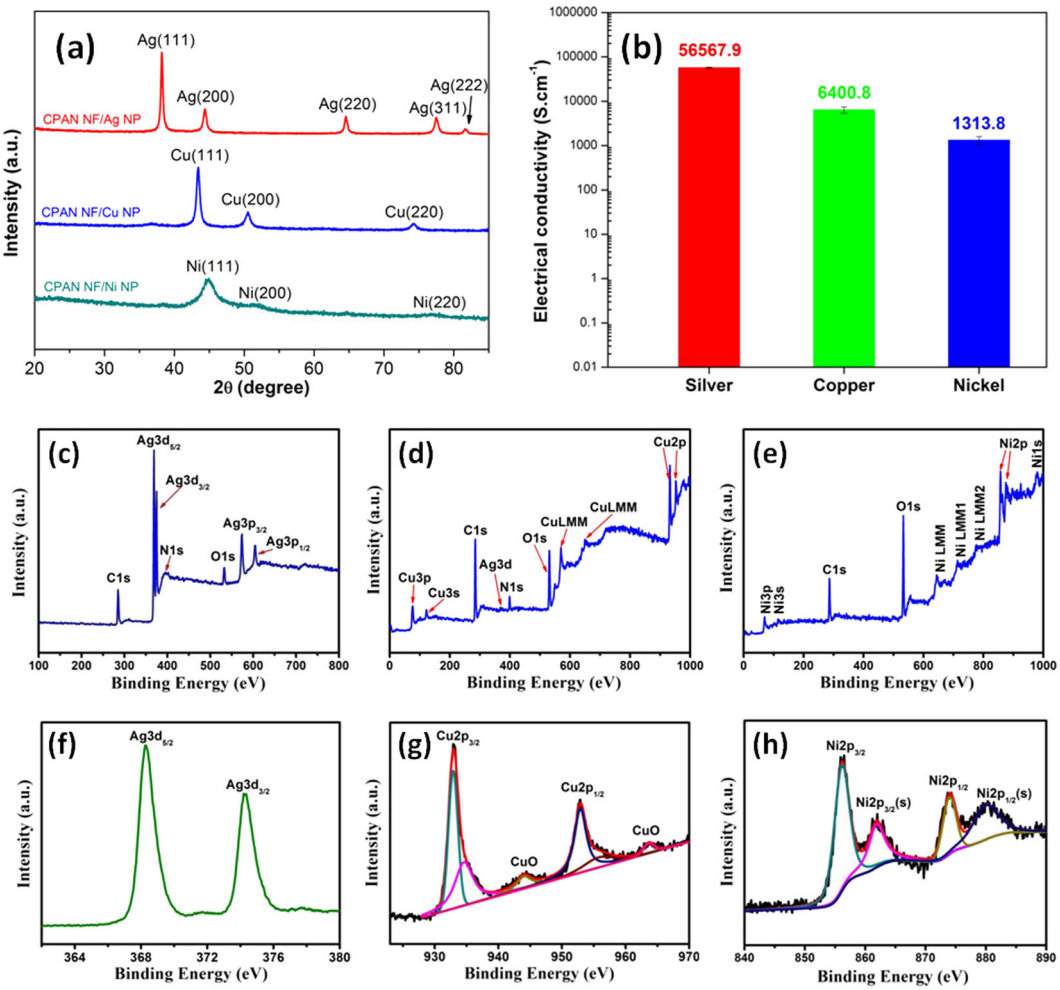

Fig. 2 Characterization and surface composition of the CPAN NF/MNP hybrid membranes. a XRD patterns of CPAN NF/MNP hybrid membranes. **b** Electrical conductivity of CPAN NF/Ag NP, CPAN NF/Cu NP and CPAN NF/Ni NP hybrid membranes. XPS wide-scan spectra of **c** CPAN NF/Ag NP, **d** CPAN NF/Cu NP, and **e** CPAN NF/Ni NP hybrid membranes corresponding to the (**f**) Ag 3d, **g** Cu 2p, and **h** Ni 2p core-level spectra

decrease in the electrical conductivities for CPAN NF/Cu NP and CPAN NF/Ni NP hybrid membranes compared to the CPAN NF/Ag NP hybrid membrane could be due to the formation of an electrically insulating metal oxide layer on the surface of Cu and Ni[24,25]. To show the exceptional electrical conductivity of the metalized NF membranes more directly, a piece of the NF mat was stabilized in a circulation circuit (Supplementary Figure S2). The metalized NF mats were able to light three light-emitting diodes (LEDs) with a total power of 3 W under an external voltage of 9 V. The brighter LED is observed for the CPAN NF/MNP hybrid membrane circuit, which is consistent with the trend of the electrical conductivity. In addition, as the deposition time of Ag NPs on the surface of CPAN NFs membrane increases, the densities of Ag NPs become larger, resulting in increased electrical conductivity (Supplementary Figure S3). When the deposition time increases from 30 min to 2 h, the electrical conductivities of the CPAN NF/Ag NP hybrid membranes increases by two orders of magnitude. Similarly, the densities of Cu and Ni NPs on the surface of the CPAN NF membrane and their electrical conductivities follow this rule (Supplementary Figures S4 and S5).

To investigate the EMI shielding ability of the prepared NF membranes, we compared CPAN NF/Ag NP, CPAN NF/Cu NP, and CPAN NF/Ni NP hybrid membranes with similar membrane thicknesses of ~35 μm in the X-band frequency range (8–12.4 GHz), Ku-band frequency range (12–18 GHz), and K-band frequency range (18–26.5 GHz), respectively. Generally, the EMI SE of conductive materials is a function of the frequency, thickness, and conductivity[26]. As shown in Fig. 3a, the EMI SE increases with the increment of frequency, which is consistent with

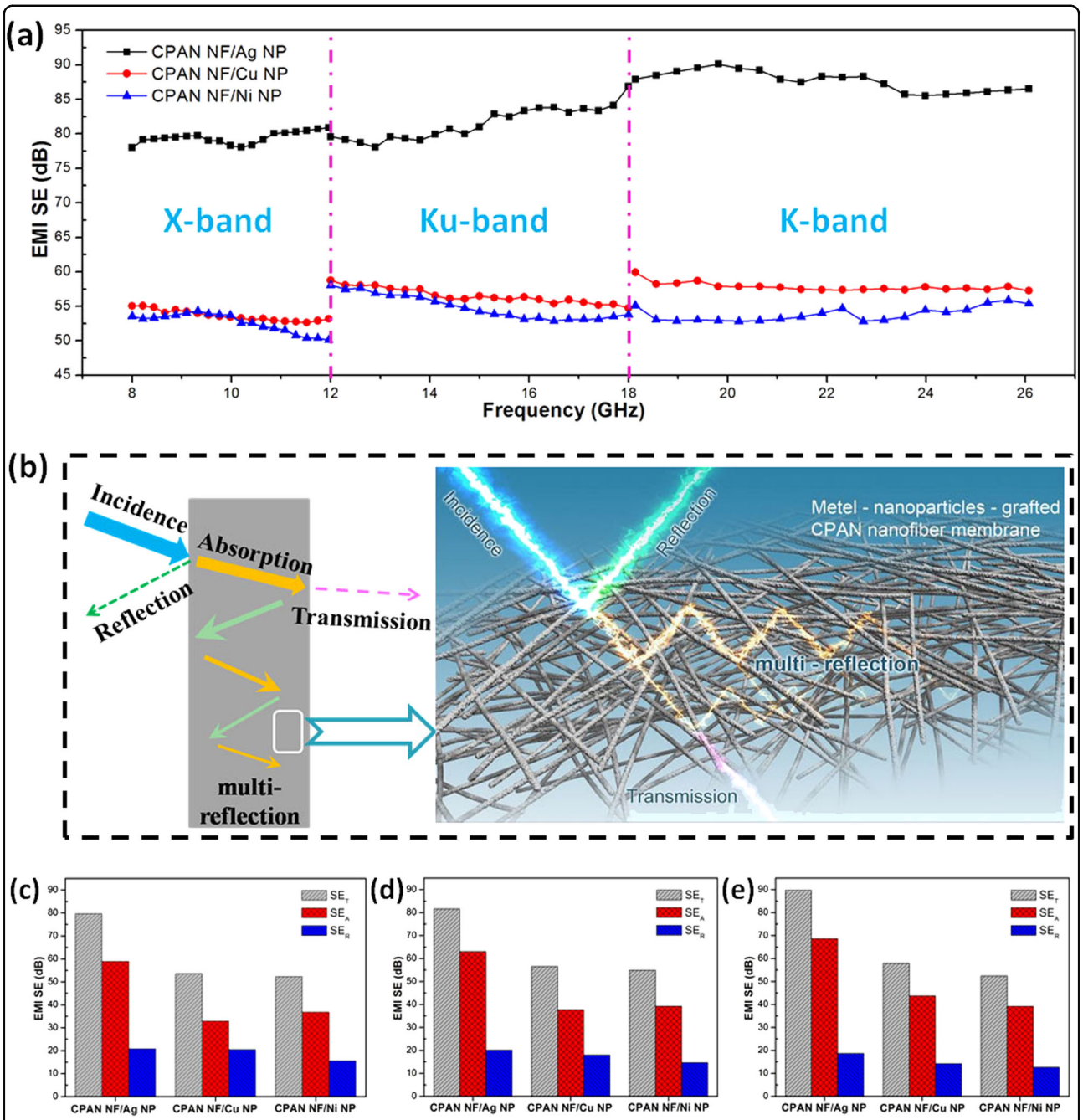

Fig. 3 EMI shielding performance of the CPAN NF/MNP hybrid membranes. a EMI SE of CPAN NF/Ag NP, CPAN NF/Cu NP, and CPAN NF/Ni NP hybrid membranes with an average thickness of ~35 μm in a broadband frequency range of 8–26.5 GHz. **b** Schematic description of the EMI shielding mechanism in the CPAN NF/MNP hybrid membranes. Total EMI SE (SE_T) and its absorption (SE_A) and reflection (SE_R) of corresponding CPAN NF/Ag NP, CPAN NF/Cu NP, and CPAN NF/Ni NP in **c** X-band, **d** Ku-band, and **e** K-band

the previous reported references[27,28]. Furthermore, the EMI SE is strongly correlated to the electrical conductivity. Consequently, CPAN NF/Ag NP hybrid membranes, with the best electrical conductivity, displayed the highest EMI SE value of approximately 83.7 dB. Based on a previous report, the EMI SE value of 83.7 dB of the prepared CPAN NF/Ag NP hybrid membrane with a thickness of ~35 μm can block more than 99.999999% of incident radiation, which means that only 0.000001% transmission of incident radiation occurs[3]. Compared with the CPAN NF/Ag NP hybrid membrane, CPAN NF/Cu NP and CPAN NF/Ni NP hybrid membranes

possessed relatively low conductivity, thus displaying decreased EMI SE values. Although the electrical conductivity of the CPAN NF/Ni NP hybrid membrane is lower than the electrical conductivity of the CPAN NF/Cu NP hybrid membrane, almost identical EMI SE values were generated. Electromagnetic wave absorption loss is well known to be the result of electric and/or magnetic dipoles in the material interacting with the radiation[3,29]. Therefore, the introduction of magnetic Ni nanoparticles on NFs as an excellent magnetic barrier shows characteristic magnetic losses, which contribute more absorption loss towards the incident EM wave[30,31]. In addition, in the X-band frequency range, higher EMI SE values were also observed at high frequencies in the Ku-band and the K-band frequency range, indicating that the prepared CPAN NF/MNP hybrid membranes possess promising applications in the EMI shielding field over a broad frequency range.

The superior EMI SE of the prepared CPAN NF/MNP hybrid membranes could be understood from a proposed mechanism shown in Fig. 3b. First, some EM waves could be directly reflected on the surface of the CPAN NF/MNP hybrid membrane due to the abundant free electrons forming surface plasmon resonance at the surface of MNPs[32,33]. Then, the remaining waves would pass through the CPAN NF/MNP hybrid membrane. When the EM waves strike the high-electron density of MNPs inside the CPAN NF/MNP hybrid membrane, the induced currents would produce ohmic losses, resulting in a drop in EM wave energy. As mentioned, many porous structures have been observed in the CPAN NF/MNP hybrid membrane. For the CPAN NF/Ag NP-90 hybrid membrane, the porosity can reach as much as 61.0 ± 1.9%. The membrane showed a relatively narrower pore size distribution in the range of 550–600 nm (Supplementary Figure S6). Therefore, the EM waves can be reflected back and forth among the NFs until they are completely absorbed in the porous NF membrane structure. To further demonstrate the relationship between the porosity and the EMI SE values, we have prepared CPAN NF/Ag NP membranes with different fiber diameters. As shown in Supplementary Figure S7, a series of CPAN NF/Ag NP-90 membranes with fiber diameters ranging from ~230 to 600 nm have been prepared by tuning the concentration of the electrospinning solution from 6 to 10%, followed by an electroless deposition process. Supplementary Figure S8 shows that the larger fiber diameter results in a higher porosity. The influence of the fiber diameters on the electrical conductivity and EMI SE of CPAN NF/Ag NP-90 with a similar membrane thickness has been investigated. The results show that there is no significant difference in the electrical conductivity. However, the sample from the 6% electrospinning solution shows the minimum electrical conductivity value, which could be due to the poor continuous metal layer on the thinner fibers compared with other thicker fibers (Supplementary Figure S9a). However, Supplementary Figure S9b shows that the sample from the 8% electrospinning solution (diameter = 368 ± 3 nm) exhibits the highest EMI SE. With the concentration of the electrospinning solution increasing from 6 to 8%, the increased EMI SE should be due to the higher porosity of the membranes. However, when the concentration of the electrospinning solution increases to more than 9%, the EMI SE values decreases slightly, which should be due to the lower percentage of metal on the surface of fibers with a larger diameter to meet the similar membrane thickness to evaluate the EMI SE performance. Generally, the total EMI SE (SE_T) is the sum of the effectiveness of absorption loss (SE_A) and reflection loss (SE_R). Reflection loss is determined by an impedance mismatch between air and shield. High conductivity exhibits a large impedance mismatch at the interface, so the reflection loss depends on the intrinsic conductivity. Absorption loss is determined by both the thickness and conductivity of the material. The average values of SE_T, SE_A, and SE_R at a wide-band frequency (8–26.5 GHz) for CPAN NF/MNP hybrid membranes were plotted in Fig. 3c–e. For the CPAN NF/Ag NP hybrid membrane, the mean values of SE_T, SE_A, and SE_R are 83.7, 63.9, and 19.8 dB, respectively. For the CPAN NF/Cu NP hybrid membrane, the mean values of SE_T, SE_A, and SE_R are 56.0, 38.4, and 17.6 dB, respectively. For the CPAN NF/Ni NP hybrid membrane, the mean values of SE_T, SE_A, and SE_R are 53.7, 39.4, and 14.3 dB, respectively. The contribution of absorption to the EMI shielding effectiveness is much larger than the contribution of reflection, so absorption loss is the dominant shielding mechanism. The results also demonstrate that with the electrical conductivity increased, both the SE_T and SE_A increased significantly, while SE_R rose only slightly. It is particularly noted that the multi-reflections are included with the absorption mechanism of the EM wave because the re-reflected waves will finally be dissipated in the form of heat in the EMI shielding materials[3]. Therefore, the multi-reflections among the CPAN NF/MNP hybrid membranes play an important role in the contribution of the excellent EMI shielding performance.

To ascertain the effect of the densities of the conductive metal on the surface of CPAN NFs, the experimental EMI SE results for the CPAN NF/MNP hybrid membrane with different electroless deposition times have been demonstrated (Fig. 4a). The EMI SE was clearly observed to increase with the increment of the electroless deposition time from 30 to 90 min, which is consistent with the trend of their electrical conductivities. The EMI SE does not change much when the electroless deposition time increases from 90 min to 2 h, indicating that the time of 90 min is sufficient to coat continuous Ag NPs with a high

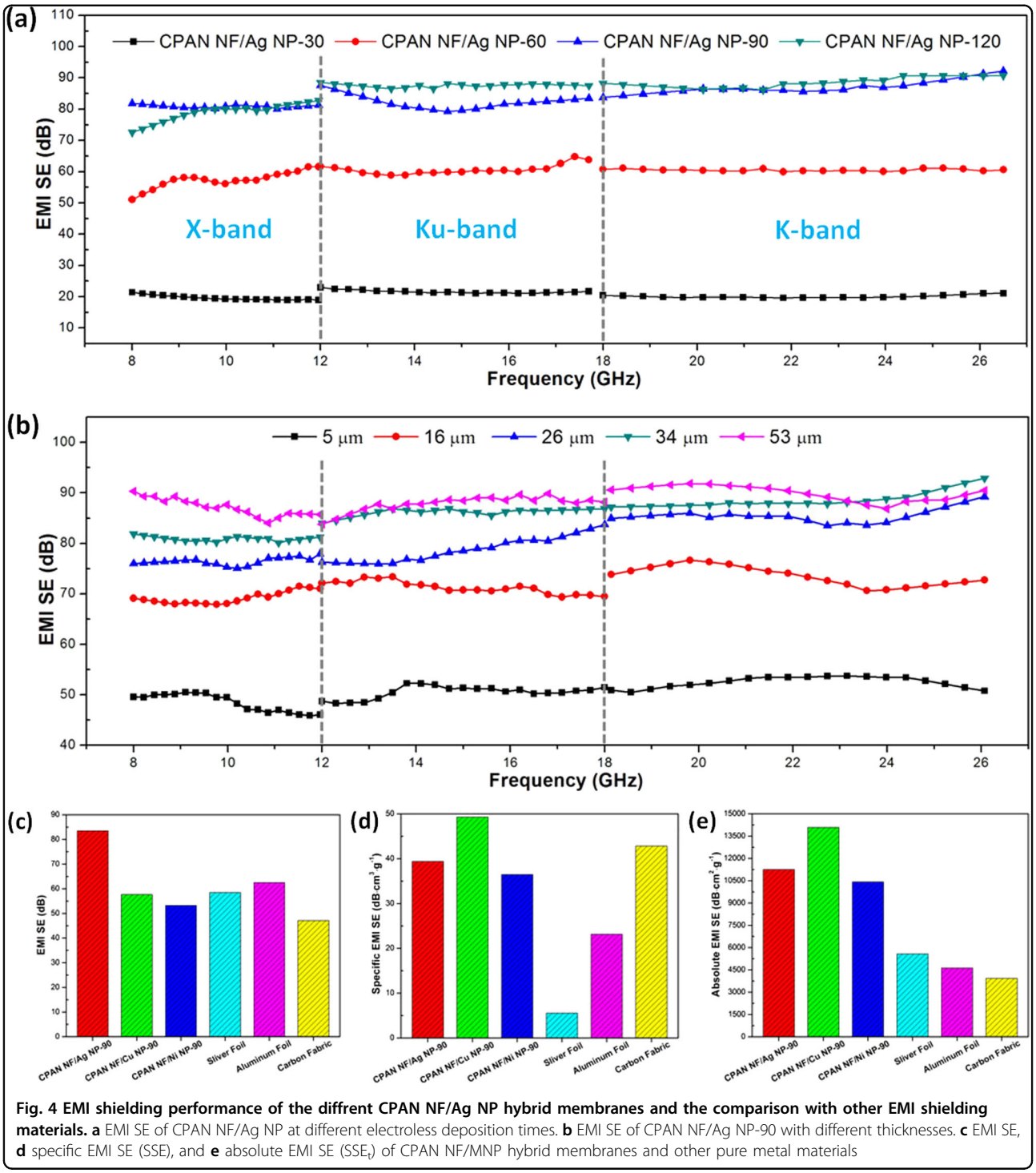

Fig. 4 EMI shielding performance of the diffrent CPAN NF/Ag NP hybrid membranes and the comparison with other EMI shielding materials. a EMI SE of CPAN NF/Ag NP at different electroless deposition times. **b** EMI SE of CPAN NF/Ag NP-90 with different thicknesses. **c** EMI SE, **d** specific EMI SE (SSE), and **e** absolute EMI SE (SSE_t) of CPAN NF/MNP hybrid membranes and other pure metal materials

density, which has been proved by the SEM images (Supplementary Figure S3c). The maximum EMI SE could reach approximately 85 dB when the electroless deposition time is 2 h. This value is among the best results for synthesized EMI shielding materials, which is consistent with the previously reported results[3]. The similar results have also been observed for the CPAN NF/Cu NP and CPAN NF/Ni NP hybrid membranes (Supplementary Figures S10 and S11). The maximum EMI SE could reach approximately 67 and 53 dB for the CPAN NF/Cu NP and CPAN NF/Ni NP hybrid membranes, respectively, with an electroless deposition time of 2 h.

In general, as long as the EMI shielding materials are thick enough, adequate shielding can be achieved.

However, thin EMI shielding membranes are necessary for their applications in the fields of aerospace, sophisticated instruments, and mobile devices due to their material economization and lightweight. Therefore, we have studied the effect of the thickness of the CPAN NF/MNP hybrid membranes on the EMI shielding performance (Fig. 4b). The average EMI SE value of the NF membrane is found to be able to increase from 50 to 90 dB by the increment of the specimen thickness from 5 to 53 μm. The increment of the EMI SE values is attributed mainly to the increment of the SE_A values (Supplementary Figure S12). An EMI SE value of 50 dB for the CPAN NF/Ag NP hybrid membranes with such a small thickness is desirable because the common commercial EMI shielding materials usually display a large thickness more than 1 mm to satisfy the commercial EMI shielding requirement (above 30 dB). To date, many materials including carbon nanotubes, graphenes, iron oxides, ferrites, and conductive metal–polymer composites have been developed as EMI shielding materials[4,18,34–36]. Foam structures of the EMI shielding materials have been widely studied to achieve lightweight characteristics for aerospace and telecommunication applications[37,38]. To compare the EMI shielding performance, specific EMI shielding effectiveness (SSE, dividing the EMI SE by the density of the sample) and absolute EMI shielding effectiveness (SSE_t, dividing SSE by the thickness of the material) are usually used because the density and thickness of the EMI shielding materials are very important to the EMI shielding performance. We have compared the SE, SSE, and SSE_t values of the prepared CPAN NF/MNP hybrid membranes with previously studied EMI shielding materials (Fig. 4c–e, Supplementary Tables S1 and S2). The results demonstrated that the SE value of the prepared CPAN NF/Ag NP hybrid membrane (deposition time 90 min) is much higher than most of the synthesized EMI shielding materials with similar or much larger thickness. However, SSE_t values of the prepared CPAN NF/MNP hybrid membranes can reach 11,254, 14,089, and 10,419 dB cm^2 g^{-1} for CPAN NF/Ag NP, CPAN NF/Cu NP, and CPAN NF/Ni NP hybrid membranes, which are superior to most of the synthesized EMI shielding materials (Supplementary Table S2). Furthermore, the SSE_t values of the prepared CPAN NF/MNP hybrid membranes are also much higher than pure silver (10 μm) and aluminum (50 μm) foils, which possess from one to more than two orders of magnitude higher electrical conductivity than CPAN NF/MNP hybrid membranes. In addition, the densities of the CPAN NF/Ag NP, CPAN NF/Cu NP, and CPAN NF/Ni NP hybrid membranes (1.17–2.12 g cm^{-3}) are much lower than the densities of the corresponding pure metals, showing their lightweight properties. In a word, the findings in this work are notable because the prepared CPAN NF/MNP hybrid EMI shielding product shows many advantages compared to the commercial EMI shielding materials such as high EMI SE (50–90 dB), low density (1.17–2.12 g cm^{-3}), small thickness (5–53 μm), facile processing, and environmental stability.

In addition, the prepared CPAN NF/MNP hybrid membranes exhibit good mechanical performance and excellent stability under mechanical deformation, demonstrating their superior flexibility properties. In this study, the amination reaction not only facilitates the formation of Ag NPs but also enhances the mechanical properties of electrospun PAN NF membranes due to the crosslinking between the amino groups and cyano groups. As shown in Fig. 5a, the tensile strength increases remarkably after the crosslinking process, where the tensile strength increases from 7.04 to 29.69 MPa and the elongation at break decreases from 27.20 to 13.20%. After the formation of Ag NPs via an electroless deposition process, the tensile strength decreases but is still higher than the tensile strength of the original PAN NF membrane (Fig. 5b). Similar results have also been observed for the CPAN NF/Cu NP and CPAN NF/Ni NP hybrid membranes (Supplementary Figure S13). In the following, we have shown that the prepared CPAN NF/MNP hybrid membranes possess excellent flexible properties. After bending for more than 2000 times, the shape and structure of the CPAN NF/MNP hybrid membranes are almost unchanged. Furthermore, we test the EMI shielding effectiveness of the CPAN NF/MNP hybrid membranes before and after repeated bending 2000 times. Only a small decrease is found after bending 2000 times, which can be attributed to the partial failure of the continuous Ag NPs on the surface of CPAN NFs (Fig. 5c). Similar results have also been observed in CPAN NF/Cu NP and CPAN NF/Ni NP hybrid membranes (Supplementary Figure S14). The excellent mechanical and flexible properties enable potential applications of the polymer NF/MNP membranes as high-performance EMI shielding materials for next-generation flexible electronic products.

Conclusions

We have reported here the fabrication of lightweight electrospun polymer NF/MNP hybrid membranes with small thickness as EMI shielding materials, exhibiting excellent electrical conductivities, outstanding shielding effectiveness and mechanical flexibility. The hybrid membranes display a shielding effectiveness as high as 90 dB in a wide frequency range (X band, Ku band, and K band) due to the unique porous structure to provide more interfaces for the microwave to reflect and scatter. More importantly, the SSE_t values of the prepared hybrid membranes can range from 10,419 to 14,089 dB cm^2 g^{-1}, superior to pure metal foils and most of the synthesized EMI shielding materials. The hybrid membranes show an excellent flexibility, offering stable EMI shielding

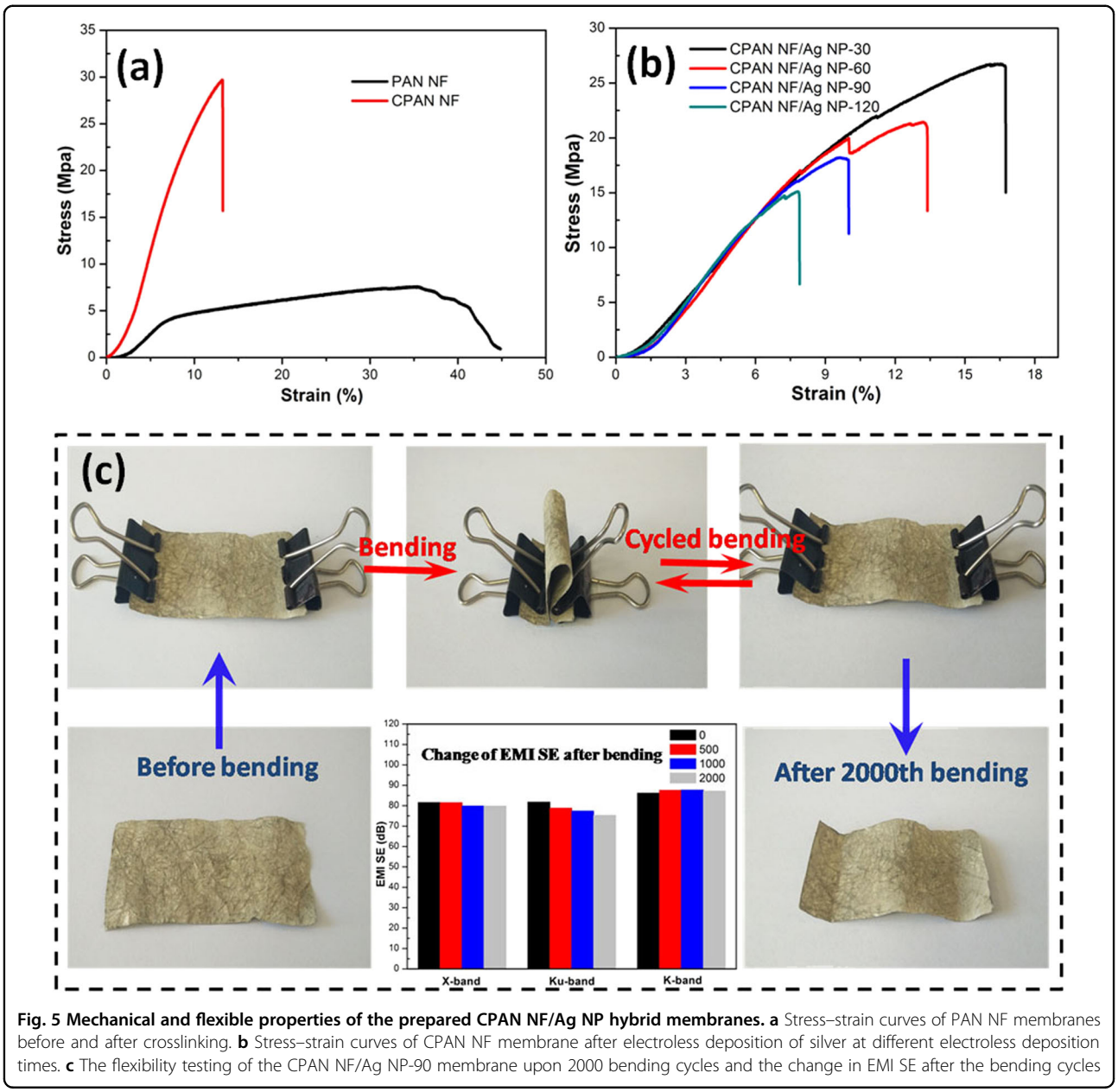

Fig. 5 Mechanical and flexible properties of the prepared CPAN NF/Ag NP hybrid membranes. a Stress–strain curves of PAN NF membranes before and after crosslinking. **b** Stress–strain curves of CPAN NF membrane after electroless deposition of silver at different electroless deposition times. **c** The flexibility testing of the CPAN NF/Ag NP-90 membrane upon 2000 bending cycles and the change in EMI SE after the bending cycles

performance under mechanical deformation. Therefore, our lightweight and flexible electrospun polymer NF/MNP hybrid membranes with a superior EMI shielding performance have potential promising applications in a large variety of fields in aerospace, defense, and smart and wearable electronics.

Acknowledgements
C.W. acknowledges the funding support from the National Natural Science Foundation of China (No. 21474043). X.F.L. thanks the National Natural Science Foundation of China (Nos. 51473065, 51773075).

Author contributions
H.J. planned and performed the experiments, collected and analyzed the data, and wrote the paper. R.Z. helped to perform the experiment and analyzed the data. N.Z. collected and analyzed the data. C.X.J. helped to perform the EIS measurements and analyzed the data. X.F.L. supervised the project, analyzed the data, and wrote the paper. C.W. supervised the project, analyzed the data, and revised the paper.

Conflict of interest
The authors declare that they have no conflict of interest.

Publisher's note
Springer Nature remains neutral with regard to jurisdictional claims in published maps and institutional affiliations.

Supplementary information is available for this paper at https://doi.org/10.1038/s41427-018-0070-1.

Received: 16 April 2018 Revised: 2 June 2018 Accepted: 17 June 2018.
Published online: 15 August 2018

References

1. Xiong, R. et al. Ultrarobust transparent cellulose nanocrystal-graphene membranes with high electrical conductivity. *Adv. Mater.* **28**, 1501–1509 (2016).
2. Li, Y., Zhao, Y., Lu, X., Zhu, Y. & Jiang, L. Self-healing superhydrophobic polyvinylidene fluoride/Fe_3O_4@polypyrrole fiber with core-sheath structures for superior microwave absorption. *Nano Res.* **9**, 2034–2045 (2016).
3. Shahzad, F. et al. Electromagnetic interference shielding with 2D transition metal carbides (MXenes). *Science* **353**, 1137–1140 (2016).
4. Yousefi, N. et al. Highly aligned graphene/polymer nanocomposites with excellent dielectric properties for high-Performance electromagnetic interference shielding. *Adv. Mater.* **26**, 5480–5487 (2014).
5. Ma, J., Zhan, M. & Wang, K. Ultralightweight silver nanowires hybrid polyimide composite foams for high-performance electromagnetic interference shielding. *ACS Appl. Mater. Interfaces* **7**, 563–576 (2014).
6. Al-Saleh, M. H., Saadeh, W. H. & Sundararaj, U. EMI shielding effectiveness of carbon based nanostructured polymeric materials: a comparative study. *Carbon* **60**, 146–156 (2013).
7. Kim, H. R., Fujimori, K., Kim, B. S. & Kim, I. S. Lightweight nanofibrous EMI shielding nanowebs prepared by electrospinning and metallization. *Compos. Sci. Technol.* **72**, 1233–1239 (2012).
8. Liu, J. et al. Hydrophobic, flexible, and lightweight MXene foams for high-performance electromagnetic-Interference shielding. *Adv. Mater.* **29**, 1702367 (2017).
9. Shen, B. et al. Microcellular graphene foam for improved broadband electromagnetic interference shielding. *Carbon* **102**, 154–160 (2016).
10. Zeng, Z. et al. Ultralight and flexible polyurethane/silver nanowire nanocomposites with unidirectional pores for highly effective electromagnetic shielding. *ACS Appl. Mater. Interfaces* **9**, 32211–32219 (2017).
11. Wang, Y. et al. Easily fabricated and lightweight PPy/PDA/AgNW composites for excellent electromagnetic interference shielding. *Nanoscale* **9**, 18318–18325 (2017).
12. Song, W. L. et al. Flexible graphene/polymer composite films in sandwich structures for effective electromagnetic interference shielding. *Carbon* **66**, 67–76 (2014).
13. Ameli, A., Nofar, M., Wang, S. & Park, C. B. Lightweight polypropylene/stainless-steel fiber composite foams with low percolation for efficient electromagnetic interference shielding. *ACS Appl. Mater. Interfaces* **6**, 11091–11100 (2014).
14. Al-Saleh, M. H. & Sundararaj, U. Electromagnetic interference shielding mechanisms of CNT/polymer composites. *Carbon* **47**, 1738–1746 (2009).
15. Chen, Z., Xu, C., Ma, C., Ren, W. & Cheng, H. M. Lightweight and flexible graphene foam composites for high-performance electromagnetic interference shielding. *Adv. Mater.* **25**, 1296–1300 (2013).
16. Zeng, Z. et al. Microstructure design of lightweight, flexible, and high electromagnetic shielding porous multiwalled carbon nanotube/polymer composites. *Small* **13**, 1701388 (2017).
17. Yang, Y., Gupta, M. C., Dudley, K. L. & Lawrence, R. W. Conductive carbon nanofiber-polymer foam structures. *Adv. Mater.* **17**, 1999–2003 (2005).
18. Zeng, Z. et al. Lightweight and anisotropic porous MWCNT/WPU composites for ultrahigh performance electromagnetic interference shielding. *Adv. Funct. Mater.* **26**, 303–310 (2016).
19. Li, X. et al. Efficient adsorption of gold ions from aqueous systems with thioamide-group chelating nanofiber membranes. *Chem. Eng. J.* **229**, 420–428 (2013).
20. Li, X., Wang, M., Wang, C., Cheng, C. & Wang, X. Facile immobilization of Ag nanocluster on nanofibrous membrane for oil/water separation. *ACS Appl. Mater. Interfaces* **6**, 15272–15282 (2014).
21. Ling, P., Li, D. & Wang, X. Supported CuO/γ-Al2O3 as heterogeneous catalyst for synthesis of diaryl ether under ligand-free conditions. *J. Mol. Catal. A* **357**, 112–116 (2012).
22. Hayez, V., Franquet, A., Hubin, A. & Terryn, H. XPS study of the atmospheric corrosion of copper alloys of archaeological interest. *Surf. Interface Anal.* **36**, 876–879 (2004).
23. Wang, J. et al. Fabrication of nanoscale NiO/Ni heterostructures as electrocatalysts for efficient methanol oxidation. *J. Mater. Chem. A* **5**, 9946–9951 (2017).
24. Aindow, M., Alpay, S. P., Liu, Y., Mantese, J. V. & Senturk, B. S. Base metal alloys with self-healing native conductive oxides for electrical contact materials. *Appl. Phys. Lett.* **97**, 152103 (2010).
25. Louzguine-Luzgin, D. V. et al. Bulk metallic glassy surface native oxide: its atomic structure, growth rate and electrical properties. *Acta Mater.* **97**, 282–290 (2015).
26. Mahmoodi, M., Arjmand, M., Sundararaj, U. & Park, S. The electrical conductivity and electromagnetic interference shielding of injection molded multi-walled carbon nanotube/polystyrene composites. *Carbon* **50**, 1455–1464 (2012).
27. Hayashida, K. & Matsuoka, Y. Electromagnetic interference shielding properties of polymer-grafted carbon nanotube composites with high electrical resistance. *Carbon* **85**, 363–371 (2015).
28. Shen, B. et al. Strong flexible polymer/graphene composite films with 3D saw-tooth folding for enhanced and tunable electromagnetic shielding. *Carbon* **113**, 55–62 (2017).
29. Singh, K. et al. Nanostructured graphene/Fe_3O_4 incorporated polyaniline as a high performance shield against electromagnetic pollution. *Nanoscale* **5**, 2411–2420 (2013).
30. Shen, B., Zhai, W., Tao, M., Ling, J. & Zheng, W. Lightweight, multifunctional polyetherimide/graphene@Fe_3O_4 composite foams for shielding of electromagnetic pollution. *ACS Appl. Mater. Interfaces* **5**, 11383–11391 (2013).
31. Song, W. L. et al. Magnetic and conductive graphene papers toward thin layers of effective electromagnetic shielding. *J. Mater. Chem. A* **3**, 2097–2107 (2015).
32. Kelly, K. L., Coronado, E., Zhao, L. L. & Schatz, G. C. The optical properties of metal nanoparticles: the influence of size, shape, and dielectric environment. *J. Phys. Chem. B* **107**, 668–677 (2003).
33. Barakat, N. A. et al. Surface plasmon resonances, optical properties, and electrical conductivity thermal hystersis of silver nanofibers produced by the electrospinning technique. *Langmuir* **24**, 11982–11987 (2008).
34. Singh, A. P. et al. Encapsulation of γ-Fe_2O_3 decorated reduced graphene oxide in polyaniline core-shell tubes as an exceptional tracker for electromagnetic environmental pollution. *J. Mater. Chem. A* **2**, 3581–3593 (2014).
35. Liu, H. et al. Preparation and the electromagnetic interference shielding in the X-band of carbon foams with Ni-Zn ferrite additive. *J. Eur. Ceram. Soc.* **36**, 3939–3946 (2016).
36. Zhang, L. et al. Mussel-inspired polydopamine coated hollow carbon microspheres, a novel versatile filler for fabrication of high performance syntactic foams. *ACS Appl. Mater. Interfaces* **6**, 18644–18652 (2014).
37. Song, Q. et al. Carbon nanotube-multilayered graphene edge plane core-shell hybrid foams for ultrahigh-performance electromagnetic-interference shielding. *Adv. Mater.* **29**, 1701583 (2017).
38. Chen, Y. et al. High-performance epoxy nanocomposites reinforced with three-dimensional carbon nanotube sponge for electromagnetic interference shielding. *Adv. Funct. Mater.* **26**, 447–455 (2016).